# Coverage Optimization With Beamsteering-Based Indoor Optical Wireless Communications

Haitham Al Satai, Bastien Béchadergue, Luc Chassagne, Wafaa Mohammed Ridha Shakir

# Coverage Optimization With Beamsteering-Based Indoor Optical Wireless Communications

Haitham AL Satai*, Bastien Béchadergue*, Luc Chassagne* and Wafaa Mohammed Ridha Shakir†
*Laboratoire d'Ingénierie des Systèmes de Versailles
Université Paris-Saclay, UVSQ, 78140 Vélizy-Villacoublay, France
Email: {haitham.al-satai, bastien.bechadergue, luc.chassagne}@uvsq.fr
†Department of Computer Systems
Al-Furat Al-Awsat Technical University, Babil, Iraq
Email: inb.wfa@atu.edu.iq

***Abstract*—Optical wireless communication (OWC) is now seen as a serious complement to radio frequency solutions, as the latter may soon face a spectrum crunch. OWC systems, however, usually rely on cells generated by fixed access points, so that they often experience a strong quality of service degradation because of frequent handover and inter-cell interference. To overcome these problems, steerable optical antennas may be used at both the infrastructure and user levels. Although such beamsteering solutions have already been explored experimentally, there seems to be no thorough comparison of the performance of such a system, especially in terms of coverage, compared to conventional solutions based on fixed antennas. This paper thus aims to provide such a comparison by simulating three scenarios ('with beamsteering', 'without beamsteering', and with 'manual orientation'), for each of which the bit error rate of a multiband carrierless amplitude phase modulation signal received by a user moving across a 20×20 m receiving plane at 0.85 m from the floor is estimated. The parameters of this source, its directivity and emission optical power, in particular, are carefully chosen to meet photobiological regulations, and their influence on the coverage is also studied. The results obtained show that beamsteering still enables, in the worst case, a threefold increase in coverage compared to scenarios where it is not or partially used.**

***Index Terms*—Beamsteering, LiFi, optical wireless communications (OWC), visible light communications (VLC)**

## I. Introduction

As radio frequency (RF) wireless communication develops, the available radio spectrum is getting closer to saturation. To address this possible spectrum crunch, optical wireless communication (OWC) has been proposed [1] and is now seen as a promising complementary solution to RF systems and a component of the sixth-generation (6G) networks due to its numerous features, including high security, speed, bandwidth, and electromagnetic interference-free operation [2]. Several OWC systems using light-emitting diodes (LED) or laser diodes have been demonstrated over the years for various applications, including indoor LiFi networking, vehicular communication, or underwater communication [3], [4].

In many studies, though, the proposed systems often rely on cell-based topologies using multiple access points (AP) bounded on the ceiling to guarantee persistent connectivity for the user equipment (UE). Albeit this topology is functional, it has several limitations. First, it is usually preferable to have large cells in order to avoid recurrent horizontal handovers, as this will increase the need for signaling at the expense of traffic transmission. However, coverage areas larger than a few square meters are difficult to achieve with fixed optical sources. The signal-to-noise ratio (SNR) and, thus, the quality of service (QoS) deteriorate rapidly as the UE moves away from the optical axis of the source and generally become very low after a few meters [5]. Moreover, each cell change results in a temporary loss of connection, which further degrades the QoS, along with the inter-cell interference.

As in RF, beamsteering has thus been proposed to enable cell-free OWC and optimize the QoS. Several studies have experimentally demonstrated tremendous throughputs in the Gbps and Tbps range [6], [7], as well as numerous methods to concretely achieve beamsteering, for example, with optical phased arrays (OPA) [8], spatial light modulators (SLMs) [9], [10], coherent-hologram [11], or micro-electro-mechanical systems (MEMS) [12]. However, to the authors' knowledge, there is no study that extensively compares the performance of an OWC system using a beamsteering solution with a more traditional cell-based system based on fixed APs. In particular, the influence of beamsteering on the spatial distribution of the bit error rate (BER) and the coverage of an OWC link has never been quantified. Consequently, this paper aims to investigate beamsteering effectiveness in optimizing the performance of an indoor infrared (IR) OWC system in terms of both BER and coverage area.

The system architecture is first described, with specific attention paid to the transmitted optical power limitations induced by photobiological safety regulations when using IR LED indoors [13]. Simulation is then employed to estimate the coverage area – defined as the zone where the BER remains below a given forward error correction (FEC) threshold [14] – under three different scenarios: 'with beamsteering', 'without beamsteering', and with a 'manual orientation' of the UE photodiode (PD) receiver. In each scenario, 34,560 symbols modulated with quadrature amplitude modulation of order $M$ ($M$-QAM) are mapped using multi-band carrierless amplitude and phase ($m$-CAP) modulation and sent by an IR LED-based AP to a UE moving around a 20×20×3 m room. Several combinations of transmitted optical power, semi-angles at half power (i.e., directivity) of the LED, and QAM orders are

tested to understand their influence on the coverage.

The results confirm the significant effect of beam steering, as it can provide coverage around three times greater than that obtained with a system where the UE is oriented manually toward a fixed AP while the transmitted optical power is just below the threshold fixed by photobiological regulations. This gain is even greater when the power is in the common range of a few watts, e.g., around fifty at 1 W, and strongly increases with the directivity of the source but decreases with $M$.

This paper is presented as follows: Section II describes the system architecture and channel modeling in detail. The results and discussion are then displayed in Section III. Finally, the main conclusions are drawn in Section IV.

## II. System Architecture and Modelling

### A. System Architecture and Channel Model

The system under study consists of an AP embedding a single IR LED mounted on the ceiling of a 20×20×3 m indoor room. At the other end of the link, a UE moves on an $x$-$y$ plane 0.85 m above the floor. Three scenarios named 'with beamsteering', 'without beamsteering', and 'manual orientation', illustrated in Fig. 1, are studied.

In the scenario 'with beamsteering', illustrated in Fig. 1(a), the AP and UE are facing each other whatever the UE position, i.e., their normal vectors $\overrightarrow{n_{AP}}$ and $\overrightarrow{n_{UE}}$ are always collinear and of opposite directions. In such a case, the angle of irradiance $\phi$ between $\overrightarrow{n_{AP}}$ and the direction of emission is null, as the angle of incidence $\psi$ between the $\overrightarrow{n_{UE}}$ and the direction of reception (i.e., $\phi = \psi = 0$). This scenario is the subject of our current study, which we intend to incorporate into future practical applications. In the scenario 'without beamsteering', represented in Fig. 1(b), the AP is pointing toward the floor, whereas the UE is pointing toward the ceiling so that whatever the UE position, we have $\phi = \psi$. Such a scenario corresponds to the typical network topology connecting a PC to an AP when using most current commercial LiFi products [15]. Finally, when 'manual orientation' is considered, the AP is oriented toward the floor, whereas the UE always faces the AP, regardless of its position, such as a user in a room always orientatating his device toward the AP to get a connection, as depicted in Fig. 1(c). In such a case, $\phi \neq \psi$ except when the UE is directly below the AP.

In this study, we aim to evaluate the performance of our system under the three previous scenarios in terms of coverage area. For this purpose, we need to simulate the current signal $y(t)$ produced by the PD in the UE from the optical signal $x(t)$ sent by the AP. According to [3], we know that:

$$y(t) = R_{\mathrm{PD}} x(t) \otimes h(t) + n(t), \tag{1}$$

where $R_{\mathrm{PD}}$ is the PD sensitivity, $h(t)$ is the impulse response of the OWC channel between the AP and the UE, and $n(t)$ is the additive white Gaussian noise (AWGN) at the PD level.

The channel impulse response $h(t)$ is, in practice, composed of a line-of-sight (LoS) component coming from the direct propagation path of length $d$ between the AP and UE, along with non-LoS (NLoS) paths coming from reflections on the walls and obstacles. However, these NLoS paths are neglected here as their contribution to $h(t)$ can be considered negligible, except at the room's edges [16]. In addition, we can consider the channel remains relatively flat up to a few tens of MHz [3], so that (1) can be approximated as:

$$y(t) = R_{\mathrm{PD}} P_t(t) H_{\mathrm{LoS}}(0) + n(t), \tag{2}$$

where $P_t(t)$ is the instantaneous transmitted optical power and $H_{\mathrm{LoS}}(0)$ is the channel direct current (DC) gain coming from the LoS propagation path between the AP and UE.

This LoS channel DC gain is commonly defined as [3]:

$$H_{\mathrm{LoS}}(0) = \begin{cases} \frac{A_{\mathrm{PD}}(m_t+1)}{2\pi d^2} \cos^{m_t}(\phi) \cos(\psi) T_f(\psi) G_c(\psi) \\ \text{if } 0 \leq \phi \leq \pi/2 \text{ and } 0 \leq \psi \leq \psi_{\mathrm{c}}, \\ 0 \text{ otherwise}, \end{cases} \tag{3}$$

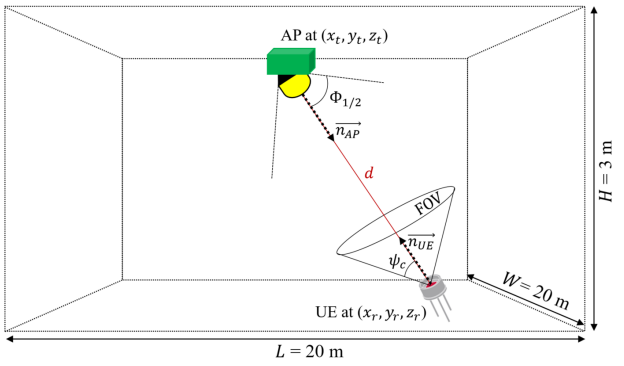


(a) Scenario 'with beamsteering' ($\phi = \psi = 0$).

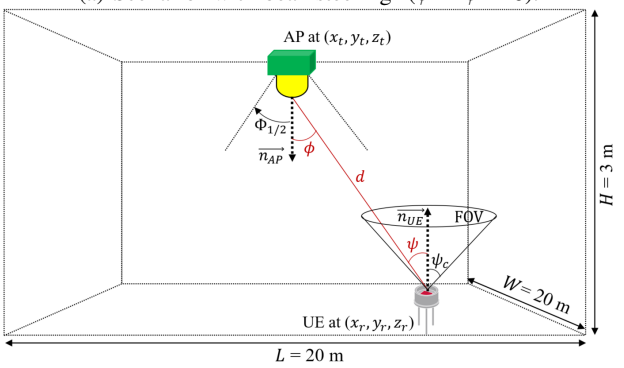


(b) Scenario 'without beamsteering' ($\phi = \psi$).

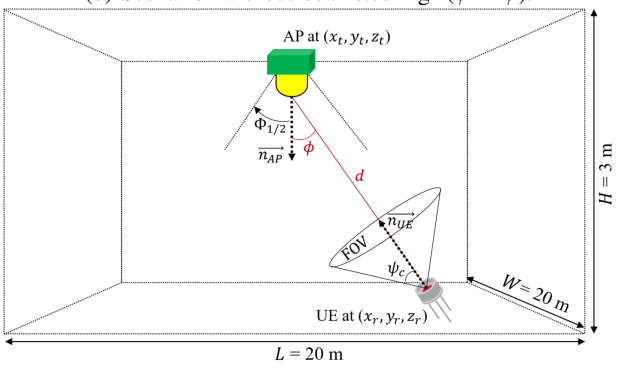


(c) Scenario with 'manual orientation' ($\phi \neq \psi$).

Fig. 1: Indoor OWC scenarios considered.

where $A_{\mathrm{PD}}$ is the sensitive area of the PD, whereas $T_f(\psi)$ and $G_c(\psi)$ represent the gains of the optical filter and optical concentrator that may be placed in front of the PD to enhance the light collection. Note that according to (3), the transmitted signal can only be collected by the PD if its angle of incidence $\psi$ is smaller than the field of view (FoV) $\psi_c$ of the UE.

According to (3), the LoS channel DC gain $H_{\mathrm{LoS}}(0)$ also depends on the directivity of the LED, which is here modeled as a generalized Lambertian emitter of order $m_t$ [3], with:

$$m_t = \frac{-\ln 2}{\ln\left(\cos\left(\Phi_{1/2}\right)\right)}, \tag{4}$$

where $\Phi_{1/2}$ is the semi-angle at half power, i.e., the angle at which the maximum optical power of the source is reduced by half. In other words, the smaller $\Phi_{1/2}$, the larger $m_t$ and the more directive the source, which, however, has implications on the optical power that can be safely transmitted.

### B. Photobiological Safety Limits

When used beyond certain limits, IR light can be hazardous to the retina and cornea of the eyes, but also the skin. To avoid these hazards, the IEC-62471 standard [13] defines irradiance and radiance exposure limits (EL) that should not be exceeded. In the majority of cases, the most restrictive EL concerns the irradiance $E_{\mathrm{IR}}$ to which the cornea can be exposed at 20 cm in the optical axis of the source, given by:

$$E_{\mathrm{IR}} = \begin{cases} 18000 \times t_{exp}^{-0.75} \text{ W.m}^{-2} & \text{when } t_{exp} \leq 1000 \text{ s}, \\ 100 \text{ W.m}^{-2} & \text{when } t_{exp} > 1000 \text{ s}, \end{cases} \tag{5}$$

with $t_{exp}$ the exposure duration. In other words, if the irradiance produced by the source is on average below 100 W.m$^{-2}$, then the source is safe. Combining (2) and (3) with $d$ = 0.20 m and a sensitive area of 1 m$^2$, we can estimate the irradiance in W.m$^{-2}$ at the receiver level for a given semi-angle at half power $\Phi_{1/2}$, and thus estimate the maximum optical power $P_{t,max}$ that an IR LED can transmit as a function of $\Phi_{1/2}$:

$$P_{t,max}(\Phi_{1/2}) = \frac{8\pi \ln\left(\cos\left(\Phi_{1/2}\right)\right)}{\ln\left(\cos\left(\Phi_{1/2}\right)\right) - \ln 2}. \tag{6}$$

The results are represented in Fig. 2 and show that $P_{t,max}$ logically decreases as the source directivity increases.

### C. $m$-CAP Data Transmission Principles

In this work, the data signal considered for BER and coverage performance evaluation is generated using an $m$-CAP modulation. $m$-CAP is a variant of CAP, where the frequency spectrum is separated into $m$ sub-bands, each utilizing a CAP modulation process to create a multi-carrier system [17]. Thus, $m$-CAP is a promising alternative to well-known and popular techniques as it preserves the features of traditional CAP while diminishing the sensitivity to non-flat channel responses and ensures lower peak-to-average power ratio (PAPR) than typical orthogonal frequency-division multiplexing (OFDM) schemes [18]. To that end, it relies on digital or analog pulse shaping filters, making it much more straightforward

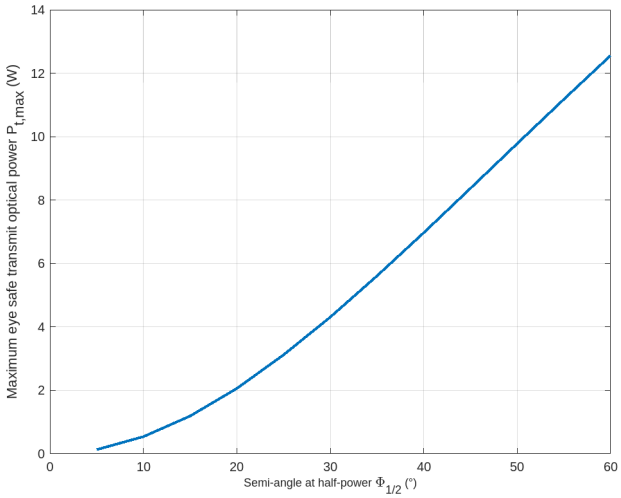


Fig. 2: Evolution of the maximum optical power $P_{t,max}$ that can be safely transmitted according to the semi-angle at half power $\Phi_{1/2}$ of the IR LED source used.

than the fast Fourier transform/inverse fast Fourier transform (FFT/IFFT) operations [19].

In theory, an $m$-CAP modulator first maps a stream of binary data over $m$ parallel streams using an $M$-QAM scheme. The resulting symbols are upsampled by a factor $N_{ss}$ compared to the initial sampling frequency $f_{samp}$ and then separated into real and imaginary (in-phase and quadrature, or I/Q) components. The $m$ I/Q pairs are finally filtered with digital or analog finite impulse response (FIR) filters of roll-off factor $\alpha$ and length $L_{\mathrm{SPAN}}$ and then summed up to build the $m$-CAP data signal. This signal spreads over a total bandwidth $B$ and is composed of $m$ sub-bands of center frequencies $f_{sc}$ and bandwidth $B_{sc}$. Then, the reverse operations are performed on the demodulator side to retrieve the binary data. Note that more details on the $m$-CAP modulation and demodulation process used here can be found in [5], where it is also specified that the overall data rate $R_b$ eventually achieved is:

$$R_b = m \log_2(M) B_{sc}. \tag{7}$$

In practice, the total signal bandwidth $B$, the number of sub-bands $m$, their center frequencies $f_{sc}$, their bandwidth $B_{sc}$, their QAM modulation order $M$, as well as the roll-off factor $\alpha$ and span $L_{\mathrm{SPAN}}$ of the FIR shaping filters can be freely adjusted to fit real-world constraints. For example, the total bandwidth $B$ has been here set to match the modulation bandwidth of an existing IR LED, which we measured at 30 MHz [20]. Then, in order to guarantee an adequate guard band between the sub-bands, as well as at low frequency to avoid interference from artificial and natural light sources, we divided the total bandwidth into $m = 15$ sub-bands of center frequencies $f_{sc} = \{2k+1\}_{k=0,\cdots,14}$ MHz, and of width $B_{sc} = 1$ MHz. In parallel, we set the FIR filters roll-off factor $\alpha$ to 0.4 and their span $L_{\mathrm{SPAN}}$ to 10 to maintain a good compromise between performance and complexity [5].

TABLE I: $m$-CAP PARAMETERS.

| Parameter | Value |
|---|---|
| Number of sub-bands ($m$) | 15 |
| Sub-bands frequencies ($f_{sc}$) | $\{2k+1\}_{k=0,\cdots,14}$ MHz |
| Sub-bands width ($B_{sc}$) | 1 MHz |
| QAM order ($M$) | 16 ($R_b$ = 60 Mbps)<br>32 ($R_b$ = 75 Mbps)<br>64 ($R_b$ = 90 Mbps)<br>128 ($R_b$ = 105 Mbps)<br>256 ($R_b$ = 120 Mbps)<br>512 ($R_b$ = 135 Mbps)<br>1024 ($R_b$ = 150 Mbps) |
| Roll-off factor ($\alpha$) | 0.4 |
| I/Q filters length ($L_{\mathrm{SPAN}}$) | 10 |
| Sampling frequency ($f_{samp}$) | 60 MHz |
| Oversampling factor ($N_{ss}$) | 10 |
| Modulation depth | 50 % |

Finally, to respect the photobiological safety limits, the $m$-CAP signal is generated with an instantaneous optical power in the range $[P_{t,max}/2, 3P_{t,max}/2]$ at the most, with $P_{t,max}$ set according to the semi-angle at half power $\Phi_{1/2}$ of the IR LED source using (6). In other words, the average optical power of the transmitted signal is at the most $P_{t,max}$ and its modulation depth is 50% so that even the maximum instantaneous emitted optical power is such that the corresponding irradiance remains below the EL defined in (5) when the exposure duration $t \leq 1000$ s. All these parameters and their values are summed up in Table I.

## III. SIMULATION RESULTS AND DISCUSSION

### A. Simulation Parameters

We simulated the system previously described in a 20×20×3 m indoor room, with an AP in the middle of the ceiling and a UE moving by steps of 0.5 m along the $x$ and $y$ directions of an $x$-$y$ reception plane 0.85 m above the floor. This simulation was conducted with MATLAB, with the objective of determining the BER performance and coverage area of the proposed system in the scenarios 'with beamsteering', 'without beamsteering', and with 'manual orientation' for different combinations of semi-angle at half power (i.e., directivity), transmitted optical power of the IR LED source and QAM order. To do this, 34,560 $M$-QAM symbols (i.e., more than $10^5$ bits of whatever $M$), modulated with $m$-CAP, were sent from the AP to the UE for each possible position on the reception plane and for each scenario. For each one of these location/scenario combinations, the received data signal was demodulated to estimate the BER. The coverage area was then estimated as the set of locations where the BER remained below the FEC threshold of $3.8 \times 10^{-3}$ [14].

Detailed information about the parameters used during the simulations is provided in Table I regarding the $m$-CAP signal and Table II regarding the geometrical and UE parameters. It may be noted that we consider the UE to be equipped with four Hamamatsu S6967 PD, from the datasheet of which the values for the FOV $\psi_{\mathrm{c}}$, the responsivity $R_{\mathrm{PD}}$ and the effective area $A_{\mathrm{PD}}$ are taken [21]. In addition, we set the power spectral density (PSD) $N_0$ of the AWGN to $10^{-21}$ following the literature [22].

TABLE II: SIMULATION PARAMETERS.

| Parameter | Value |
|---|---|
| Room dimensions ($L \times W \times H$) | $20 \times 20 \times 3$ m |
| [$x$,$y$,$z$] coordinates of the AP | [0,0,0] |
| Height of the UE | 0.85 m (i.e. $h$ = 1.65 m) |
| FOV of the PD ($\psi_{\mathrm{c}}$) | 85° [21] |
| Responsivity of the PD ($R_{\mathrm{PD}}$) | 0.63 A/W [21] |
| Effective area of the PD ($A_{\mathrm{PD}}$) | 105.6 $\mathrm{mm}^2$ [21] |
| Optical filter gain ($T_f$) | 1 (no filter used) |
| Optical concentrator gain ($G_c$) | 1 (no concentrator used) |
| Number of $M$-QAM symbols sent | 34560 |
| Noise PSD ($N_0$) | $10^{-21}$ [22] |

### B. System Performance When $P_t = P_{t,max}$

In order to understand not only the interest of beamsteering on the BER and coverage performance but also the influence of the semi-angle at half power $\Phi_{1/2}$ (i.e., directivity) and optical power $P_t$ of the IR LED source within photobiological limits, we first set $P_t$ to the safety limit whatever $\Phi_{1/2}$ using (6), i.e., $\forall \Phi_{1/2} \in [5°, 60°], P_t = P_{t,max}\left(\Phi_{1/2}\right)$. We then evaluated the performance of each scenario under this condition for multiple values of QAM order $M$.

Figure 3 shows the evolution of the coverage area against $M$ for different values of $\Phi_{1/2}$. The coverage area curves exhibit the same behavior, whatever the source directivity. Note that most curves are superimposed on each other, so they cannot be clearly distinguished. This is because, on the one hand, the AP and UE are always aligned thanks to beamsteering, and on the other hand, the irradiance at the UE level and, thus, the optical power collected by its PD is independent of $\Phi_{1/2}$ as the transmitted optical power is set to meet the constraint given by (6) whatever the value of $\Phi_{1/2}$.

We also observe that increasing the QAM-order $M$ results in a gradual reduction in coverage, from around 120 $\mathrm{m}^2$ to 5 $\mathrm{m}^2$ (over a total of 400 $\mathrm{m}^2$ for a 20×20 m reception plane). This is because when $M$ increases, the resulting QAM constellation of each sub-band gets denser and, thus, more sensitive to noise. Since the noise has a constant PSD $N_0$, this results in higher BER levels and, therefore, in lower coverage.

Figure 4 then compares the coverage area ensured in each of the three scenarios studied against the semi-angle at half power for a fixed QAM order ($M$ = 16). It shows that 'with beamsteering', the coverage remains around 120 $\mathrm{m}^2$ whatever $\Phi_{1/2}$ whereas it is at the most 40 $\mathrm{m}^2$ with 'manual orientation', hence providing a three-fold increase in coverage while consuming much less electrical power for light emission (the electrical power consumed by the beamsteering system remains, however, an open question).

It also shows that the coverage 'without beamsteering' and with 'manual orientation' follows a similar trend, starting from near zero at $\Phi_{1/2} = 5°$ and then increasing gradually with $\Phi_{1/2}$. The 'manual orientation' provides, however, better coverage at large semi-angle at half power (e.g., 40 $\mathrm{m}^2$ vs. 20 $\mathrm{m}^2$ at $\Phi_{1/2} = 60°$), as the alignment of the receiver's normal with the direction of reception allows, in this case, to exploit a larger effective sensitive area of the PD, and thus to collect more optical power in all points of the reception plane.

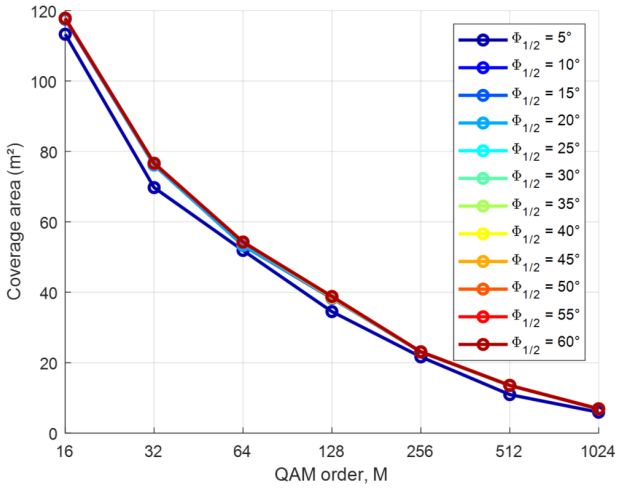


Fig. 3: Evolution of the coverage area as a function of the QAM order $M$ 'with beamsteering', and for different semi-angles at half power $\Phi_{1/2}$, when $P_t = P_{t,max}$.

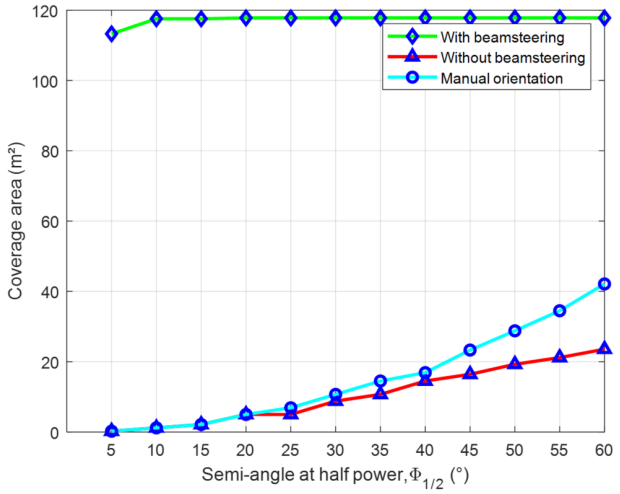


Fig. 4: Evolution of the coverage area as a function of the semi-angle at half power $\Phi_{1/2}$ in the scenarios 'with beamsteering', 'without beamsteering' and with 'manual orientation', where the QAM order $M$ = 16.

### C. System Performance When $P_t$ = 1 W

In practice, the OWC system may not be able to adjust its transmitted optical power with $\Phi_{1/2}$ to be at the exact photobiological safety EL. Therefore, we consider here a fixed transmitted optical power $P_t$ of 1 W and study the influence of beamsteering, semi-angle at half power $\Phi_{1/2}$ and QAM order $M$ on the coverage performance. Figure 5 shows the resulting coverage 'with beamsteering' as a function of $M$ and $\Phi_{1/2}$.

We can clearly see that with a 5° semi-angle at half power, the room is entirely covered for QAM orders up to 32. However, such cases are actually not acceptable in terms of photobiological safety, as the minimum value for $\Phi_{1/2}$ when $P_t$ = 1 W is around 13°. Therefore, when focusing our

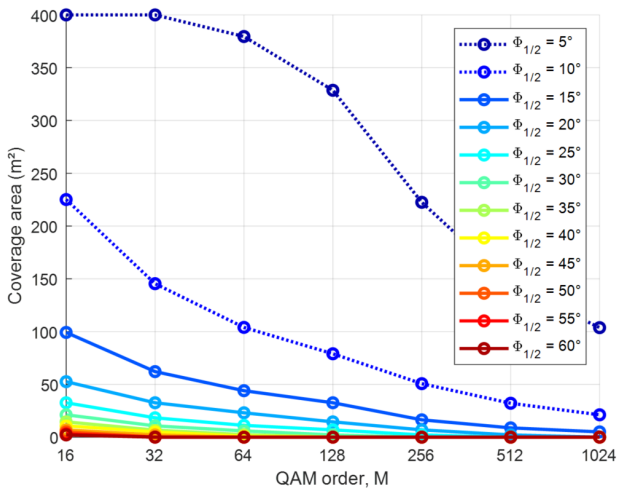


Fig. 5: Evolution of the coverage area as a function of the QAM order $M$ and semi-angles at half power ($\Phi_{1/2}$), in the scenario 'with beamsteering' and with $P_t$ = 1 W. The dotted curves correspond to cases where the safety standards are not respected.

attention to the curves where $\Phi_{1/2} \geq 15°$, we can observe that the coverage area decreases with $M$ whatever $\Phi_{1/2}$, for the same reasons as previously. However, we can also observe that the coverage decreases with $\Phi_{1/2}$ whatever the QAM order. This is because the transmitted optical power is now fixed so it is more and more diffused as $\Phi_{1/2}$ gets larger. This results in the decrease of the optical power received by the UE, and thus in a received signal with lower SNR and higher BER.

Then, Fig. 6(a) compares the evolution of the coverage area for the three scenarios versus $\Phi_{1/2}$ and for a fixed QAM order ($M$ = 16). We can clearly observe that the coverage is much larger 'with beamsteering' than in the other two cases, especially with directive sources. Keeping in mind that cases where $\Phi_{1/2} \leq 13°$ may cannot be considered for safety reasons, we can see that the maximum coverage 'with beamsteering' is 100 m$^2$ whereas it is only 3 m$^2$ in the other two cases. However, we can also notice that the interest of beamsteering remains strongly limited with diffused sources, as can be seen by comparing the coverage in all scenarios when $\Phi_{1/2} > 30°$. In such cases, the gain in received optical power provided by beamsteering is indeed overcompensated by the fact that only a small fraction of the transmitted optical power propagates along the direction of emission whereas most of the power is diffused in other directions.

Finally, Fig. 6(b) shows that the coverage remains pretty similar 'without beasmteering' and with 'manual orientation'. The interest of 'manual orientation' is even less visible here, with $P_t$ = 1 W, than when $P_t$ is set at the safety limit (see Fig. 4). This comes again from the fact that a large fraction of the fixed transmitted optical power is diffused and cannot be collected by the UE, even when turning it toward the direction of emission. In this regard, we can actually observe that an optimum semi-angle at half power appears around 30°. It

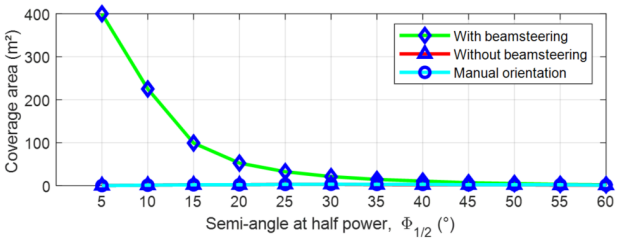


(a) All scenarios.

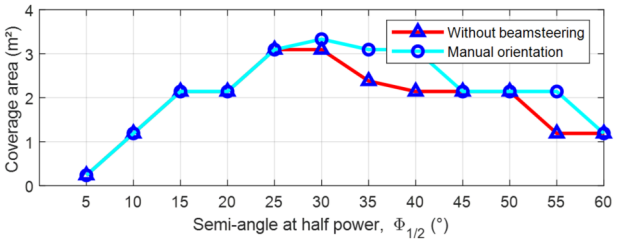


(b) Scenarios 'without beamsteering' and with 'manual orientation'.

Fig. 6: Coverage area versus semi-angle at half power $\Phi_{1/2}$ when $P_t$ = 1 W and $M$ = 16.

corresponds to the case where the optical signal is focused enough to be collected by the UE and diffused enough to support displacements of the UE.

## IV. Conclusion

This paper studies the influence of beamsteering on the coverage area provided by an indoor OWC system. This system is composed of an AP based using a single IR LED, operated within photobiological safety limits, as an emitter, and a UE moving across a 20×20 m reception plane at 0.85 m from the floor. It shows that whether the transmitted optical power $P_t$ is set to the safety limit depending on the semi-angle at half power $\Phi_{1/2}$, or to a fixed value whatever $\Phi_{1/2}$, beamsteering does bring a considerable gain in the coverage area, compared to the cases where it is not used ('without beamsteering') or partially used ('manual orientation'). It also shows that when $P_t$ is fixed, the lower $\Phi_{1/2}$ (i.e. the more directive the source), the better in terms of coverage, hence confirming a useful design rule for such systems. However, such a rule should be followed carefully as for any given transmitted optical power, $\Phi_{1/2}$ should not be below a certain limit set by photobiological safety regulations. In addition, more directive sources may be more sensitive to misalignment and displacements, hence requiring more accurate beamsteering. Therefore, there could be an optimal source directivity depending on all these constraints, the analysis of which is left to future work. A further intention is to verify the above results experimentally in similar scenarios.

## Acknowledgment

This work was supported by the French National Research Agency (ANR) through the project SAFELiFi under grant ANR-21-CE25-0001-01. It was also based upon work from COST Action NEWFOCUS CA19111, supported by COST (European Cooperation in Science and Technology).

## References

[1] T. Cogalan, and H. Haas, "Why would 5G need optical wireless communications?," in *2017 IEEE 28th Annu. Int. Symp. on Personal, Indoor, and Mobile Radio Communications (PIMRC)*, 2017, pp. 1-6.

[2] N. Chi, Y. Zhou, Y. Wei, and F. Hu, "Visible light communication in 6G: Advances, challenges, and prospects", *IEEE Veh. Technol. Mag.*, vol. 15, no. 4, pp. 93-102, Dec. 2020.

[3] Z. Ghassemlooy, L. N. Alves, S. Zvanovec, and M. A. Khalighi, Eds., *Visible Light Communications: Theory and Applications*. Boca Raton, FL, USA: CRC press, 2017.

[4] P. A. Hoeher, J. Sticklus, and A. Harlakin, "Underwater Optical Wireless Communications in Swarm Robotics: A Tutorial," *IEEE Commun. Surveys Tuts.*, vol. 23, no. 4, pp. 2630-2659, Fourthquarter 2021.

[5] L. Shi, B. Béchadergue, L. Chassagne, and H. Guan, "Joint Visible Light Sensing and Communication Using $m$-CAP Modulation," *IEEE Trans. Broadcast.*, 2022.

[6] T. Koonen *et al.*, "High-Capacity Optical Wireless Communication Using Two-Dimensional IR Beam Steering," *J. Lightw. Technol.*, vol. 36, no. 19, pp. 4486-4493, Oct. 2018.

[7] R. Singh *et al.*, "Design and Characterisation of Terabit/s Capable Compact Localisation and Beam-Steering Terminals for Fiber-Wireless-Fiber Links," *J. Lightw. Technol.*, vol. 38, no. 24, pp. 6817–6826, Dec. 2020.

[8] P. F. McManamon *et al.*, "A review of phased array steering for narrow-band electrooptical systems," *Proc. IEEE*, vol. 97, no. 6, pp. 1078-1096, May. 2009.

[9] F. Feng, I. H. White, and T. D. Wilkinson, "Holographic beam steering a directly modulated two-electrode high brightness tapered laser diode for optical wireless communications," *Asia Communications and Photonics Conf. (ACP)*, pp. 1-3, Nov. 2012.

[10] S. M. Kim, and S. M. Kim, "Performance improvement of visible light communications using optical beamforming," *5th Int. Conf. on Ubiquitous and Future Networks (ICUFN)*, pp. 362-365, July. 2013.

[11] T. A. Tran, and D. C. Kim, "LED holographic beam-steering for visible-light communications," *IEEE Globecom Workshops (GC Wkshps)*, pp. 1099–1102, Dec. 2013.

[12] T. K. Chan *et al.*, "Optical beamsteering using an 8× 8 MEMS phased array with closed-loop interferometric phase control," *Opt. Express*, vol. 21, no. 3, pp. 2807-2815, Feb. 2013.

[13] *Photobiological safety of lamps and lamp systems*, IEC-62471:2006, International Electrotechnical Commission, Geneva, Switzerland, 2006.

[14] *Forward Error Correction for High Bit-Rate DWDM Submarine Systems*, Recommendations ITU-T G.975.1, International Telecommunication Union, Geneva, Switzerland, Feb. 2004.

[15] B. Béchadergue, B. Azoulay, "An industrial view on LiFi challenges and future," *12th Int. Symp. on Communication Systems, Networks and Digital Signal Processing (CSNDSP)*, pp. 1-6, Jul. 2020.

[16] L. An, H. Shen, J. Wang, Y. Zeng, and R. Ran, "Energy Efficiency Optimization for MIMO Visible Light Communication Systems," *IEEE Wireless Commun. Lett.*, vol. 9, no. 4, pp. 452–456, Apr. 2020.

[17] M. I. Olmedo *et al.*, "Multiband Carrierless Amplitude Phase Modulation for High Capacity Optical Data Links," *J. Lightw. Technol.*, vol. 32, no. 4, pp. 798-804, Feb. 2014.

[18] M.-A. Khalighi, S. Long, S. Bourennane, and Z. Ghassemlooy, "PAM- and CAP-Based Transmission Schemes for Visible-Light Communications," *IEEE Access*, vol. 5, pp. 27002-27013, 2017.

[19] X. Li *et al.*, "A Full-Digital $M$-CAP Receiver With Synchronisation and Adaptive Blind Equalisation for Visible Light Communications," *J. Lightw. Technol.*, vol. 40, no. 8, pp. 2409-2426, Apr. 2022.

[20] *DS191 LUXEON IR Domed Line Product Datasheet*, Lumileds Holding B.V., Haarlemmermeer, The Netherlands, 2022.

[21] *Si PIN Photodiodes S2506/S6775/S6967 Series*, Hamamatsu, Bridgewater, NJ, USA, 2021.

[22] Y. Hei, Y. Kou, G. Shi, W. Li, and H. Gu, "Energy-Spectral Efficiency Tradeoff in DCO-OFDM Visible Light Communication System," *IEEE Trans. Veh. Technol.*, vol. 68, no. 10, pp. 9872–9882, Oct. 2019.